

Effect of resonant magnetic perturbations on secondary structures in drift-wave turbulence

M. Leconte¹ and P. H. Diamond^{1,2}

¹WCI Center for Fusion Theory, NFRI, Daejeon, Korea

²CMTFO and CASS, UCSD, California 92093, USA

(Received 6 June 2011; accepted 23 June 2011; published online 29 August 2011)

Recent experiments showed a decrease of long range correlations during the application of resonant magnetic perturbations (RMPs) [Y. Xu *et al.*, Nucl. Fusion **51**, 063020 (2011)]. This finding suggests that RMPs damp zonal flows. To elucidate the effect of the RMPs on zonal structures in drift wave turbulence, we construct a generalized Hasegawa-Wakatani model including RMP fields. The effect of the RMPs is to induce a linear coupling between the zonal electric field and the zonal density gradient, which drives the system to a state of electron radial force balance for large RMP amplitude. A predator-prey model coupling the primary drift wave dynamics to the zonal modes evolution is derived. This model has both turbulence drive and RMP amplitude as control parameters and predicts a novel type of transport bifurcation in the presence of RMPs. The novel regime has a power threshold which increases with RMP amplitude as $\gamma_c \sim [\frac{\delta B_z}{B}]^2$. © 2011 American Institute of Physics. [doi:10.1063/1.3610547]

I. INTRODUCTION

The H-mode regime is the targeted operating regime for ITER. It is characterized by a transport barrier at the plasma edge. However, edge localized modes (ELMs) threaten the lifespan of the device wall and divertor plates, imposing an excessive heat load on the plasma-facing components.

Several experiments show suppression or mitigation of ELMs using resonant magnetic perturbations (RMPs).^{1–5} RMPs are static magnetic perturbations of the equilibrium magnetic field, produced by a set of external coils. The suppression of ELMs has a resonant character and the application of RMPs induces a collapse of the density pedestal, termed “density pump-out.”

Although experiments are successful in mitigating ELMs, the mechanism leading to this mitigation is yet poorly understood. Global 3D numerical simulations of resistive ballooning mode (RBM) show that RMPs stabilize relaxation oscillations of a transport barrier, which have characteristics similar to type-III ELMs (Refs. 6 and 7). Recently, experiments in L-mode indicate that zonal flows (ZFs) are damped during RMP activation.⁸ This paper aims at providing a qualitative description of the role of RMPs in the zonal flow damping and to give an insight into a quantitative description of this effect by, for example, scaling laws. Aspects of this work are still ongoing. RMP effects on shear flows were previously investigated numerically and analytically, in the framework of the RBM turbulence model.⁹ In presence of RMPs, the flux-surface averaged equations had two RMP-related terms, a linear zonal flow damping term $A_{\delta B}$ and a magnetic-flutter diffusive heat flux $Q_{\delta B}$.

In the framework of a drift wave (DW) turbulence model in presence of RMPs, we show that while similar terms are present, additional effects appear. In contrast to the RBM model, these terms linearly couple the evolution of zonal density and zonal potential, globally referred to as

zonal modes (ZMs), through the generalized Ohm’s law. The physical mechanism is the following: without RMPs, on mesoscales, the perpendicular dynamics decouple from the parallel dynamics: zonal flows (e.g., polarization electric fields) are spontaneously generated, through the Reynolds stress, so as to ensure ambipolarity (i.e., charge balance) on mesoscales. Their growth is limited only by neoclassical drag. In presence of RMPs, on mesoscales, the perpendicular dynamics does not decouple from the parallel dynamics, due to the radial scattering of electrons along perturbed magnetic field lines. We define zonal modes as $m=0, n=0$ long-range correlated fluctuations of potential and density. Long-range correlated fluctuations of potential, also known as zonal flows, are routinely observed in fusion devices.¹⁰ Although $m=0, n=0$ long-range correlated fluctuations in the density have not been observed in tokamaks, experiments on a small stellarator showed that such long-range correlations in density coexisted, and were approximately in-phase with zonal flows.¹¹ The essential physics of zonal flows is rooted in electric field generation due to ambipolarity breaking. In particular, the net (integrated) vorticity “charge” Q in an annulus—equivalent to the mean zonal shear on the scale of the region’s thickness evolves according to

$$\frac{dQ}{dt} = - \int dA \langle \tilde{v}_x \tilde{\rho}_{pol} \rangle |_{r1}^{r2}, \quad (1)$$

where $\tilde{\rho}_{pol} \sim \rho^2 \nabla_{\perp}^2 \phi$ is the polarization charge density. Thus, the effective shear is determined by the flux of polarization charge. However, $\langle \tilde{v}_x \tilde{\rho}_{pol} \rangle$ is just the Reynolds force, so the link between ambipolarity and zonal flows is evident. As we will demonstrate, introducing a radial RMP field creates a second channel for ambipolarity breaking via radial electron current flow along B_{radial} . Stochasticity of the magnetic field is not essential. The upshot is that with RMPs,

$$\frac{dQ}{dt} = - \int dA \left[\langle \tilde{v}_x \tilde{\rho}_{pol} \rangle + \left(\frac{\delta B_r}{B_0} \right)^2 D_{\parallel} \frac{\partial}{\partial x} (\langle \phi \rangle - \langle n \rangle) \right] \Big|_{r_1}^{r_2}, \quad (2)$$

where the brackets refer to zonal averages, $D_{\parallel} = \frac{v_{th}^2}{\nu_{ei}}$. Thus, flux of polarization charge and radial electron flow can now compete, so the ambipolarity is substantially altered. The bottom line of this radial electron current is a coupled evolution of zonal potential $\langle \phi \rangle$ and zonal density $\langle n \rangle$ described by

$$\frac{\partial}{\partial t} \langle n \rangle = - \frac{\partial}{\partial x} \langle \tilde{v}_x \tilde{n} \rangle + D_{RMP} \frac{\partial^2}{\partial x^2} (\langle n \rangle - \langle \phi \rangle), \quad (3)$$

$$\rho_s^2 \left(\frac{\partial}{\partial t} + \mu \right) \frac{\partial^2}{\partial x^2} \langle \phi \rangle = - \rho_s^2 \frac{\partial}{\partial x} \langle \tilde{v}_x \nabla_{\perp} \tilde{\phi} \rangle + D_{RMP} \frac{\partial^2}{\partial x^2} (\langle n \rangle - \langle \phi \rangle). \quad (4)$$

This is the fundamental dynamical system describing zonal mode evolution with RMP. Here, $D_{RMP} = D_{\parallel} (\delta B_x / B_0)^2$. This paper is devoted to the derivation and analysis of this system. The analysis proceeds by a modulational stability analysis and the derivation of an evolution equation for the drift wave turbulence intensity via wave kinetics. A variety of simplifications are used to condense these to a dynamical systems model, namely an extension of the familiar predator-prey equations, now extensively modified by RMP coupling. That model is then analysed in detail.

The remainder of this paper is organized as follows. Section II presents the model and the basic physics and formulates and executes the modulational stability analysis for zonal modes. Section III formulates and implements the reduced dynamical system predator-prey model, analyzes the system with the RMP, determines the new fixed points, and discusses their transitions and stability. Section IV summarizes the results and presents a final discussion.

II. MODEL

In presence of RMPs, the Hasegawa-Wakatani equations, describing drift-wave turbulence can be generalized to

$$\frac{\partial n}{\partial t} + \{ \phi, n \} = - \nabla_{\parallel}^2 (n - \phi), \quad (5)$$

$$\rho_s^2 \frac{\partial \nabla_{\perp}^2 \phi}{\partial t} + \{ \phi, \rho_s^2 \nabla_{\perp}^2 \phi \} = - \nabla_{\parallel}^2 (n - \phi), \quad (6)$$

where the parallel gradient ∇_{\parallel} includes the effect of RMP magnetic perturbations

$$\nabla_{\parallel} = \nabla_{\parallel 0} + \tilde{\nabla}_{\parallel}. \quad (7)$$

Here, the parallel gradient perturbation is given (in the vacuum approximation) by

$$\tilde{\nabla}_{\parallel} = \{ \tilde{\psi}_{vac}, \cdot \}, \quad (8)$$

$\tilde{\psi}_{vac}$ denotes the magnetic flux generated by the RMP-producing coils. In the following, we use the notation $\tilde{\psi} = \tilde{\psi}_{vac}$.

Upon flux-surface averaging, Eqs. (5) and (6) yield

$$\frac{\partial}{\partial t} \langle n \rangle + \frac{\partial}{\partial x} \langle \tilde{v}_x \tilde{n} \rangle = D_{\parallel} \langle \nabla_{\parallel 0} \tilde{\nabla}_{\parallel} (n - \phi) \rangle + \tilde{\nabla}_{\parallel} \nabla_{\parallel 0} \langle n - \phi \rangle + D_{\parallel} \langle \tilde{\nabla}_{\parallel} \tilde{\nabla}_{\parallel} (n - \phi) \rangle, \quad (9)$$

$$\rho_s^2 \frac{\partial}{\partial t} \nabla_{\perp}^2 \langle \phi \rangle + \mu \rho_s^2 \nabla_{\perp}^2 \langle \phi \rangle + \rho_s^2 \frac{\partial}{\partial x} \langle \tilde{v}_x \nabla_{\perp}^2 \tilde{\phi} \rangle = D_{\parallel} \langle \nabla_{\parallel 0} \tilde{\nabla}_{\parallel} (n - \phi) + \tilde{\nabla}_{\parallel} \nabla_{\parallel 0} (n - \phi) \rangle + D_{\parallel} \langle \tilde{\nabla}_{\parallel} \tilde{\nabla}_{\parallel} (n - \phi) \rangle. \quad (10)$$

The flux-surface average is defined as $\langle \dots \rangle = \iint \dots dy dz$, where y and z denote, respectively, the poloidal and toroidal directions of a fusion device. We have added a collisional drag μ due to represent neoclassical flow-friction, given by

$$\mu \sim \frac{\nu^*}{1 + (\nu^*)^2}, \quad (11)$$

with ν^* the collisionality.

To study secondary mesoscale zonal mode dynamics, we focus on the quadratic term of the particle and momentum magnetic-flutter fluxes, and can drop the terms involving $\nabla_{\parallel 0}$, so that Eqs. (9) and (10) reduce to

$$\frac{\partial}{\partial t} \langle n \rangle + \frac{\partial}{\partial x} \langle \tilde{v}_x \tilde{n} \rangle = D_{\parallel} \left\langle k_y^2 \tilde{\psi} \frac{\partial}{\partial x} \left(\tilde{\psi} \frac{\partial}{\partial x} (n - \phi) \right) \right\rangle, \quad (12)$$

$$\rho_s^2 \left(\frac{\partial}{\partial t} + \mu \right) \frac{\partial^2}{\partial x^2} \langle \phi \rangle + \rho_s^2 \frac{\partial^2}{\partial x^2} \langle \tilde{v}_x \nabla_{\perp}^2 \tilde{\phi} \rangle = D_{\parallel} \left\langle k_y^2 \tilde{\psi} \frac{\partial}{\partial x} \left(\tilde{\psi} \frac{\partial}{\partial x} (n - \phi) \right) \right\rangle. \quad (13)$$

As usual, poloidal and toroidal symmetries of the zonal modes are assumed a priori. The quantities $\langle \tilde{v}_x \tilde{n} \rangle$ and $\langle \tilde{v}_x \nabla_{\perp}^2 \tilde{\phi} \rangle$ are, respectively, the (convective) particle flux and vorticity flux, where the latter is linked to the Reynolds stress via the Taylor identity

$$\langle \tilde{v}_x \nabla_{\perp}^2 \tilde{\phi} \rangle = \frac{\partial}{\partial x} \langle \tilde{v}_x \tilde{v}_y \rangle. \quad (14)$$

Assuming the zonal perturbations of density and potential to be slowly varying in space, averaging of small (micro) scales gives

$$\frac{\partial}{\partial t} \langle n \rangle = - \frac{\partial}{\partial x} \langle \tilde{v}_x \tilde{n} \rangle + D_{RMP} \frac{\partial^2}{\partial x^2} (\langle n \rangle - \langle \phi \rangle), \quad (15)$$

$$\rho_s^2 \left(\frac{\partial}{\partial t} + \mu \right) \frac{\partial^2}{\partial x^2} \langle \phi \rangle = - \rho_s^2 \frac{\partial}{\partial x} \langle \tilde{v}_x \nabla_{\perp}^2 \tilde{\phi} \rangle + D_{RMP} \frac{\partial^2}{\partial x^2} (\langle n \rangle - \langle \phi \rangle). \quad (16)$$

Here, the coupling parameter D_{RMP} is given by

$$D_{RMP} = D_{\parallel} \sum_k k_y^2 |\psi_k|^2. \quad (17)$$

Note that $D_{RMP} = D_{\parallel} \langle (\frac{\delta B_x}{B})^2 \rangle \simeq \chi_{\parallel} \langle (\frac{\delta B_x}{B})^2 \rangle$ is very close to the effective cross-field heat conductivity induced by the external RMP fields. Equations (15) and (16) state that the

RMP linearly couples the zonal density and zonal potential evolution (n.b. recall zonal potential is the zonal flow stream function), in contrast to the familiar $D_{RMP} \rightarrow 0$ limit, in which the coupling is only implicit (i.e., nonlinear). Equations (15) and (16) have two characteristic time-scales, namely γ_{ZF}^{-1} and $(\frac{D_{RMP}}{\rho_s^2})^{-1}$. Here, γ_{ZF}^{-1} is a typical zonal flow time scale in the absence of the RMP, i.e., the inverse of a modulational growth-rate $\gamma_{ZF} = \gamma_{ZF}(\langle \tilde{v}^2 \rangle)$, and $(\frac{D_{RMP}}{\rho_s^2})^{-1}$ is a characteristic diffusion time along the perturbed field lines. Hence, zonal mode dynamics varies depending on $\alpha_{ZF} = \frac{D_{RMP}}{\gamma_{ZF} \rho_s^2}$, much like collisional drift wave dynamics bifurcates into distinct regimes for different values of $\frac{k_{\parallel}^2 D_{\parallel}}{\omega}$. This analogy is developed further in Table I. Clearly, for $\alpha_{ZF} \ll 1$, the zonal flow is determined as usual by the competition between Reynolds force and frictional damping, while for $\alpha_{ZF} \gg 1$, the zonal modes tend toward a state with $\langle n \rangle \simeq \langle \phi \rangle$, which corresponds to electron radial force balance.

In fact, in the strong-RMP limit $\alpha_{ZF} \rightarrow +\infty$, adiabaticity is restored on mesoscales: $\langle n \rangle = \langle \phi \rangle$ and an equation similar to the Hasegawa-Mima equation is obtained

$$\begin{aligned} \frac{\partial}{\partial t} \left(-\rho_s^2 \frac{\partial^2 \langle \phi \rangle}{\partial x^2} + \langle \phi \rangle \right) + \frac{\partial}{\partial x} \langle \tilde{v}_x \tilde{n} \rangle \\ = \rho_s^2 \frac{\partial}{\partial x} \langle \tilde{v}_x \nabla_{\perp}^2 \tilde{\phi} \rangle + \mu \rho_s^2 \frac{\partial^2 \langle \phi \rangle}{\partial x^2}. \end{aligned} \quad (18)$$

This equation states that the zonal potential vorticity is conserved, up to dissipation (neoclassical friction μ), and nonlinear energy transfers from particle and vorticity flux. Note that $\int dx (\langle \phi \rangle - \rho_s^2 \frac{\partial^2 \langle \phi \rangle}{\partial x^2})$ —the radially integrated potential vorticity is conserved up to dissipation and boundary terms.

One clear consequence of the $\langle \phi \rangle$, $\langle n \rangle$ coupling induced by D_{RMP} is that the zonal flow will be damped by particle transport. A physical perspective on the dynamics of the zonal mode system for RMP may be gained by considering local ambipolarity breaking or equivalently the dynamics of total polarization charge Q . In the absence of RMP and other magnetic fluctuations, it is straightforward to show that the volume-integrated vorticity Q in an annulus of surface

area A and thickness l_{\perp} (n.b. l_{\perp} corresponds to x), evolves according to

$$\frac{dQ}{dt} = - \int dA dl_{\perp} \frac{\partial}{\partial l_{\perp}} \langle \tilde{v}_x \tilde{\sigma}_{pol} \rangle, \quad (19)$$

where $\tilde{\sigma}_{pol} = \nabla_{\perp}^2 \tilde{\phi}$ is the volume polarization charge density. Thus,

$$\frac{dQ}{dt} = - \int dA \langle \tilde{v}_x \tilde{\sigma}_{pol} \rangle|_{l_1}^{l_2} \quad (20)$$

is simply the net change in polarization charge content in a given region $l_1 \leq r \leq l_2$ due to the flux of vorticity thru that region. Thus, the mean zonal shear on the scale $\Delta l = l_2 - l_1$ is determined by the competition between the differential flux of polarization charge and the decay of net polarization charge, equivalent to zonal flow damping. With magnetic fluctuations, either external or spontaneous, a second mechanism of local ambipolarity breakdown is possible via the flow of current (i.e., electrons) along radially tilted field lines. In that case,

$$\frac{dQ}{dt} = - \int dA [\langle \tilde{v}_x \tilde{\sigma}_{pol} \rangle - \langle B_x j_{\parallel} \rangle]|_{l_1}^{l_2}. \quad (21)$$

The two terms have opposite signs, since Q is an ion polarization charge while j_{\parallel} is carried by electrons. With RMP,

$$\langle B_x j_{\parallel} \rangle = \langle B_r \rangle \langle j_{\parallel} \rangle + \langle \tilde{B}_x \tilde{j}_{\parallel} \rangle. \quad (22)$$

Here, \tilde{B}_x and \tilde{j}_{\parallel} correspond to the usual electromagnetic fluctuations (i.e., with high frequency time variation), while $\langle B_x \rangle$ refers to the static radial RMP field and $\langle j_{\parallel} \rangle$ is the radial electron current along the tilted RMP field. This radial current exhibits structure on mesoscales. Since

$$j_{\parallel} = -\frac{1}{\eta} \nabla_{\parallel} (\phi - n), \quad (23)$$

then

$$\langle j_{\parallel} \rangle = -\frac{1}{\eta} \frac{\langle B_x \rangle}{B_0} \frac{\partial}{\partial x} (\langle \phi \rangle - \langle n \rangle), \quad (24)$$

Since,

$$\nabla_{\parallel} = \frac{\partial}{\partial z} + \frac{\mathbf{B}}{B_0} \cdot \nabla_{\perp}. \quad (25)$$

Thus, we see that

$$\begin{aligned} \frac{dQ}{dt} = - \int dA \left[\langle \tilde{v}_x \tilde{\sigma}_{pol} \rangle + \left(\frac{\langle B_x \rangle}{B_0} \right)^2 D_{\parallel} \frac{\partial}{\partial x} (\langle \phi \rangle - \langle n \rangle) - \langle \tilde{B}_x \tilde{j}_{\parallel} \rangle \right]_{l_1}^{l_2} \\ = - \int dA \left[\langle \tilde{v}_x \tilde{\sigma}_{pol} \rangle - \langle \tilde{B}_x \tilde{j}_{\parallel} \rangle + D_{RMP} \frac{\partial}{\partial x} (\langle \phi \rangle - \langle n \rangle) \right]_{l_1}^{l_2}. \end{aligned} \quad (26)$$

Note that for $\tilde{B}_x, \tilde{j}_{\parallel} \rightarrow 0$ (i.e., electrostatic turbulence), this in essence recovers Eq. (16), while for $D_{RMP} \rightarrow 0$, we have (without assumption regarding Ohm's law)

TABLE I. Analogy between the linear Hasegawa-Wakatani model and zonal modes with RMPs.

	Linear H-W model	Zonal modes with RMPs [Eqs. (33) and (34)]
Coupling parameter	$\frac{D_{\parallel} k_{\parallel 0}^2}{\omega_k}$	$\frac{D_{RMP} \rho_s^{-2}}{\gamma_q}$
Strong coupling	$\frac{D_{\parallel} k_{\parallel 0}^2}{\omega_k} \gg 1$	$\frac{D_{RMP} \rho_s^{-2}}{\gamma_q} \gg 1$
	adiabatic electrons drift waves	electron force balance $\langle E_r \rangle \simeq \frac{\partial}{\partial r} \langle n \rangle$
Weak coupling	$\frac{D_{\parallel} k_{\parallel 0}^2}{\omega_k} \ll 1$	$\frac{D_{RMP} \rho_s^{-2}}{\gamma_q} \ll 1$
	fluid electrons convective cell modes	modified zonal flows

$$\frac{dQ}{dt} = - \int dA [\langle \tilde{v}_x \tilde{\sigma}_{pol} \rangle - \langle \tilde{B}_x \tilde{j}_{\parallel} \rangle]_{l_1}^2. \quad (27)$$

In this case, the Taylor identity can be applied to *both* fluxes to obtain

$$\frac{dQ}{dt} = - \int dA \frac{\partial}{\partial l_{\perp}} [\langle \tilde{v}_x \tilde{v}_y \rangle - \langle \tilde{B}_x \tilde{B}_y \rangle]_{l_1}^2, \quad (28)$$

so the net change in charge content is just the net Reynolds force differential and the Maxwell force differential across the layer. For Alfvén waves or “Alfvénized” turbulence, $\frac{dQ}{dt}$ vanishes. A corresponding approach may be used to derive an expression for the total particle content of the layer, which is equivalent to Eq. (15). Thus, we see that the principal effect of the RMP on zonal modes—especially zonal flows—is to introduce a second mechanism for (local) ambipolarity breaking which can compete against the familiar one of flux of polarization charge. This second mechanism necessarily couples a standard Ohm law for electrostatic drift waves with zonal potential and density perturbations.

Now, we face the nettlesome problem of actually *calculating* something. To this end, we consider the modulational stability of a zonal potential (i.e., flow) and density perturbation in a background of ambient drift wave turbulence. As usual, the zonal modes have radial wave number q and frequency Ω_q while the drift waves have wave vector \mathbf{k} and frequency $\omega_{\mathbf{k}}$, with $|q| \ll |\mathbf{k}|$ and $\Omega_q \ll \omega_{\mathbf{k}}$. The calculation employs standard procedures, as described in Ref. 10.

Exploiting the scale separation, we introduce modulations (denoted by a “ δ ”) of the particle flux and Reynolds stress as

$$\begin{pmatrix} \delta\Gamma \\ \delta\Pi \end{pmatrix} = \begin{pmatrix} \frac{\delta\Gamma}{\delta\langle n \rangle} & \frac{\delta\Gamma}{\delta\langle \phi \rangle} \\ \frac{\delta\Pi}{\delta\langle n \rangle} & \frac{\delta\Pi}{\delta\langle \phi \rangle} \end{pmatrix} \begin{pmatrix} \langle n \rangle \\ \langle \phi \rangle \end{pmatrix}, \quad (29)$$

with the notation $\Gamma = \langle \tilde{v}_x \tilde{n} \rangle$, $\Pi = \langle \tilde{v}_x \tilde{v}_y \rangle$.

Applying a Fourier transform with radial wavenumber q , the system can be cast into matrix form

$$M_q \frac{d}{dt} \begin{pmatrix} \delta n_q \\ \delta \phi_q \end{pmatrix} + A_q \begin{pmatrix} \delta n_q \\ \delta \phi_q \end{pmatrix} = 0, \quad (30)$$

where the matrix A_q is given by

$$A_q = \begin{pmatrix} iq \frac{\delta\Gamma}{\delta n_q} + D_{RMP} q^2 & iq \frac{\delta\Gamma}{\delta \phi_q} - D_{RMP} q^2 \\ q^2 \rho_s^2 \frac{\delta\Pi}{\delta n_q} - D_{RMP} q^2 & q^2 \rho_s^2 \frac{\delta\Pi}{\delta \phi_q} + D_{RMP} q^2 + \mu q^2 \rho_s^2 \end{pmatrix}. \quad (31)$$

The mass matrix M_q is

$$M_q = \begin{pmatrix} 1 & 0 \\ 0 & q^2 \rho_s^2 \end{pmatrix}. \quad (32)$$

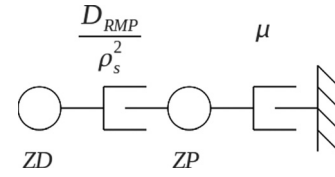


FIG. 1. Analogy between zonal modes linear dynamics and coupled dampers.

A. Linear dynamics

First, without considering the effects of particle flux and Reynolds stress, the dynamics of the system (30) corresponds to that of asymmetrically-coupled dampers [Fig. 1]

$$\frac{d}{dt} \delta n_q = -\mu_{\delta B} q^2 \rho_s^2 (\delta n_q - \delta \phi_q), \quad (33)$$

$$-q^2 \rho_s^2 \left(\frac{d}{dt} + \mu \right) \delta \phi_q = -\mu_{\delta B} q^2 \rho_s^2 (\delta n_q - \delta \phi_q), \quad (34)$$

where we define the coupling parameter $\mu_{\delta B}$ as

$$\mu_{\delta B} = \frac{D_{RMP}}{\rho_s^2 \gamma_{ZF}} = \frac{D_{\parallel}}{\rho_s^2 \gamma_{ZF}} \sum_{\mathbf{k}} k_y^2 |\psi_{\mathbf{k}}|^2. \quad (35)$$

Note that an estimate of the coupling parameter can be obtained using the linewidth of ZF modulations $\Delta\omega$

$$\mu_{\delta B} \sim \frac{D_{RMP}}{\rho_s^2 \Delta\omega}. \quad (36)$$

The asymmetry in the coupling, clearly visible on Fig. 1, stems from the fact that zonal potential is *collisionally damped* due to neoclassical friction μ , whereas zonal density is not. Note, however, that zonal density is non-linearly damped due to turbulent particle diffusivity, but this is outside the linear analysis.

An analogy can be made between the structure of Eqs. (33) and (34) and that of the equations for linear drift-waves [Table I]. Particularly, the strong-RMP limit $\frac{\gamma_q \rho_s^2}{D_{RMP}} \rightarrow 0$ is similar to the adiabatic regime $\frac{\omega_{\mathbf{k}}}{D_{\parallel} k_{\parallel}^2} \rightarrow 0$ of the linear drift-waves. There are two differences between Eqs. (33) and (34) and linear drift waves: the first difference is the presence of neoclassical friction μ and the second one is the absence of a real frequency. However, these differences do not kill the analogy.

The linear analysis yields two branches, a weakly-damped branch (+) and a strongly-damped branch (−), with damping rates given by

$$\begin{aligned} \gamma_{q0}^{\pm} = & -\frac{1}{2} (\mu + \mu_{\delta B}) \\ & + q^2 \rho_s^2 \mu_{\delta B} \pm \frac{1}{2} \sqrt{(\mu + \mu_{\delta B} - q^2 \rho_s^2 \mu_{\delta B})^2 + 4q^2 \rho_s^2 \mu_{\delta B}^2}. \end{aligned} \quad (37)$$

In the weak-coupling limit $\frac{\mu_{\delta B}}{\mu} \ll 1$, expression (37) simplifies to

$$\gamma_{q0}^+ \sim -\frac{\mu_{\delta B}}{\mu} q^2 \rho_s^2 \mu + \frac{\mu_{\delta B}^2}{\mu^2} q^2 \rho_s^2 \mu, \quad \text{for } \frac{\mu_{\delta B}}{\mu} \ll 1, \quad (38)$$

$$\gamma_{q0}^- \sim -\left(1 + \frac{\mu_{\delta B}}{\mu}\right) \mu - \frac{\mu_{\delta B}^2}{\mu^2} q^2 \rho_s^2 \mu, \quad \text{for } \frac{\mu_{\delta B}}{\mu} \ll 1. \quad (39)$$

From the limiting expressions (38) and (39), we see that the (+) branch corresponds to the zonal density branch, while the (-) branch corresponds to the zonal potential branch.

B. Modulation of particle flux and Reynolds stress by zonal modes

We now consider weakly non-adiabatic drift-waves, which can be linearly unstable. Neglecting direct RMP effect on the drift-waves, the density perturbation can be expressed in terms of the potential perturbation

$$n_k = (1 - ih)\phi_k, \quad \text{with } h = \frac{\omega_*}{D_{\parallel} k_{\parallel 0}^2} \ll 1, \quad (40)$$

where h denotes the adiabaticity parameter and $k_{\parallel 0}$ the unperturbed parallel wave-number. Therefore, for weakly non-adiabatic drift waves, the particle flux and Reynolds stress are given by

$$\Gamma = \sum_k h k_y \epsilon, \quad (41)$$

$$\Pi = \sum_k k_x k_y \epsilon, \quad (42)$$

with $\epsilon = |\varphi_k|^2$ the turbulence intensity. The modulation of the particle flux and Reynolds stress by zonal density and by zonal potential (e.g., by zonal flows) are then given by

$$\frac{\delta \Gamma}{\delta n_q} = \sum_k \frac{1}{2} h v_g \frac{\delta \Omega}{\delta n_q}, \quad (43)$$

$$\frac{\delta \Gamma}{\delta \phi_q} = \sum_k \frac{1}{2} h v_g \frac{\delta \Omega}{\delta \phi_q}, \quad (44)$$

$$\frac{\delta \Pi}{\delta n_q} = \sum_k \frac{1}{2} v_g \frac{\delta \Omega}{\delta n_q}, \quad (45)$$

$$\frac{\delta \Pi}{\delta \phi_q} = \sum_k \frac{1}{2} v_g \frac{\delta \Omega}{\delta \phi_q}, \quad (46)$$

where the radial group velocity v_g of drift waves and the potential enstrophy density Ω are given by

$$v_g = -\frac{2k_x k_y \rho_s^2}{(1 + k_{\perp}^2 \rho_s^2)^2} v_*, \quad (47)$$

$$\Omega = (1 + k_{\perp}^2 \rho_s^2)^2 \epsilon. \quad (48)$$

Here, we are exploiting the fact that the wave action density given by

$$N = \frac{\epsilon}{\omega_k} \propto \Omega, \quad (49)$$

for drift waves, is an adiabatic invariant and hence, conserved for mesoscale modulations.

This allows us to use the wave kinetic formalism to calculate the modulations $\frac{\delta \Omega}{\delta \phi_q}$.

The coupled evolution equations of zonal density and zonal potential, Eqs. (15) and (16), are now given by

$$\begin{aligned} \frac{d}{dt} \delta n_q + D_T q^2 \delta n_q + iq \sum_k h \frac{k_y^2}{(1 + k_{\perp}^2 \rho_s^2)^2} \\ \times \left(\frac{\delta \Omega}{\delta n_q} \delta n_q + \frac{\delta \Omega}{\delta \phi_q} \delta \phi_q \right) + q^2 D_{RMP} (\delta n_q - \delta \phi_q) = 0, \end{aligned} \quad (50)$$

$$\begin{aligned} q^2 \rho_s^2 \frac{d}{dt} \delta \phi_{\omega_{Dopp}} + q^2 \rho_s^2 \mu \delta \phi_q + q^2 \rho_s^2 \sum_k \frac{k_x k_y^2}{(1 + k_{\perp}^2 \rho_s^2)^2} \\ \times \left(\frac{\delta \Omega}{\delta n_q} \delta n_q + \frac{\delta \Omega}{\delta \phi_q} \delta \phi_q \right) - q^2 D_{RMP} (\delta n_q - \delta \phi_q) = 0, \end{aligned} \quad (51)$$

where $D_T \sim \epsilon$ denotes the turbulent particle diffusivity. Here, we use the fact that the modulation of D_T is weak compared to D_T , due to considerations of spectral symmetry.

The wave kinetic equation (WKE) for the response of the wave population density to the total refractive modulations reads^{12,13}

$$\frac{\partial}{\partial t} \delta N + v_g \frac{\partial}{\partial x} \delta N + |\gamma_k| \delta N = \frac{\partial}{\partial x} (\omega_k + \omega_{Dopp}) \frac{\partial}{\partial k_x} \langle \Omega \rangle, \quad (52)$$

where $|\gamma_k|$ models relaxation effects, and the drift-wave frequency ω_k and Doppler frequency ω_{Dopp} are given by

$$\omega_k = \frac{k_y v_{*e}}{1 + k_{\perp}^2 \rho_s^2}, \quad (53)$$

$$\omega_{Dopp} = k_y v_{\mathbf{E} \times \mathbf{B}}. \quad (54)$$

The underlying physics is that these two frequencies are modulated radially on mesoscales, and so induce a refraction of the linear drift waves, expressed on the r.h.s. of Eq. (52). The electron diamagnetic drift is perturbed by the zonal density

$$v_{*e} = v_{*e0} + \delta v_{*e}. \quad (55)$$

Noting that δN is proportional to $\delta \Omega$, we then have

$$\begin{aligned} \frac{\partial}{\partial t} \delta \Omega + v_g \frac{\partial}{\partial x} \delta \Omega + |\gamma_k| \delta \Omega \\ = k_y \left(\frac{1}{1 + k_{\perp}^2 \rho_s^2} \frac{\partial}{\partial x} \delta v_{*e} + \frac{\partial}{\partial x} \delta v_{\mathbf{E} \times \mathbf{B}} \right) \frac{\partial}{\partial k_x} \langle \Omega \rangle. \end{aligned} \quad (56)$$

We observe that in addition to the usual zonal $\mathbf{E} \times \mathbf{B}$ shear, there is a shear in the electron diamagnetic zonal flow. This diamagnetic flow shear is calculated as

$$\frac{\partial}{\partial x} \delta v_{*e} = -\frac{\partial^2}{\partial x^2} \delta n. \quad (57)$$

The zonal $\mathbf{E} \times \mathbf{B}$ shear is, as usual

$$\frac{\partial}{\partial x} v_{\mathbf{E} \times \mathbf{B}} = \frac{\partial^2}{\partial x^2} \delta\phi. \quad (58)$$

The coupled system of Eqs. (50) and (51) finally becomes

$$\begin{aligned} \frac{d}{dt} \delta n_q + D_T q^2 \delta n_q + i b_q (\delta\phi_q - (1-c)\delta n_q) \\ - D_{RMP} q^2 (\delta\phi_q - \delta n_q) = 0, \end{aligned} \quad (59)$$

$$\begin{aligned} \frac{d}{dt} \delta\phi_q + \mu \delta\phi_q - a_q (\delta\phi_q - (1-c)\delta n_q) \\ + \frac{D_{RMP}}{\rho_s^2} (\delta\phi_q - \delta n_q) = 0. \end{aligned} \quad (60)$$

Here, the coefficients a_q , b_q , and c are

$$a_q = -q^2 \sum_{\mathbf{k}} \frac{k_x k_y^2}{(1 + k_{\perp}^2 \rho_s^2)^2} R_q \frac{\partial \langle \Omega \rangle}{\partial k_x} \geq 0, \quad (61)$$

$$b_q = a_q \sum_{\mathbf{k}} h \frac{q}{k_x}, \quad (62)$$

$$c = \sum_{\mathbf{k}} \frac{k_{\perp}^2 \rho_s^2}{1 + k_{\perp}^2 \rho_s^2}, \quad (63)$$

where the resonance function R_q is defined by

$$R_q = \frac{|\gamma_k|}{q^2 \gamma_g^2 + |\gamma_k|^2} \sim \tau, \quad (64)$$

with τ as the spectral response correlation time.

It is straightforward to show that the coupled evolution of zonal density and zonal potential Eqs. (59) and (60) has a zonal frequency, in addition to the zonal growth rate. The analogy with linear drift waves given in the linear analysis [Table I] can be pushed further, in a quasilinear analysis: as the real frequency of linear drift waves entails their propagation, both poloidally and radially, the real frequency of zonal modes, i.e., ‘‘zonal waves,’’ entails their radial propagation. This is familiar from the case of geodesic acoustic modes which are zonal shear layers which propagate radially on account of their finite frequency and polarization effects. From Eqs. (30) and (31), we see that the real frequency, and hence radial propagation, stems from the particle flux modulation.

In the following, we neglect the radial propagation of zonal modes, since our main goal here is to describe the local dynamics of zonal flow energy with RMPs, e.g., we use the approximation

$$b_q \rightarrow 0. \quad (65)$$

With this approximation, the system (59) and (60) reduces to

$$\frac{d}{dt} \delta n_q + \mu_T q^2 \rho_s^2 \delta n_q - \mu_{\delta B} q^2 \rho_s^2 (\delta\phi_q - \delta n_q) = 0, \quad (66)$$

$$\begin{aligned} \frac{d}{dt} \delta\phi_q + \mu \delta\phi_q - a_q (\delta\phi_q - (1-c)\delta n_q) \\ + \mu_{\delta B} (\delta\phi_q - \delta n_q) = 0, \end{aligned} \quad (67)$$

where the quantity μ_T is given by

$$\mu_T = \frac{D_T}{\rho_s^2 \gamma_{ZF}}, \quad (68)$$

and $\mu_{\delta B}$ is given by expression (35).

Without RMPs, e.g., $\mu_{\delta B} \rightarrow 0$, we see from Eqs. (66) and (67) that zonal density and zonal potential decouple and their growth rate is, respectively

$$\gamma_q^- \sim -\mu_T q^2 \rho_s^2, \quad \text{for } \mu_{\delta B} \rightarrow 0, \quad (69)$$

$$\gamma_q^+ \sim a_q - \mu, \quad \text{for } \mu_{\delta B} \rightarrow 0. \quad (70)$$

Hence, without RMPs, drift waves destabilize only the zonal potential, and zonal density is damped, so we recover standard zonal flow dynamics. This explains the predominance of zonal flows in absence of RMPs. The dynamics is more complex, in the presence of RMPs, as will be shown in Sec. II C.

C. Growth-rate of the zonal modes

The growth-rates of the zonal modes, as described by Eqs. (66) and (67), are given by

$$\gamma_q^{\pm} = \frac{1}{2} (a_q - (\mu + \mu_{\delta B}) - q^2 \rho_s^2 (\mu_T + \mu_{\delta B})) \pm \frac{\sqrt{\Delta}}{2}, \quad (71)$$

where the discriminant Δ can be cast into the following form:

$$\begin{aligned} \Delta = (a_q - (\mu + \mu_{\delta B}) + q^2 \rho_s^2 (\mu_T + \mu_{\delta B}))^2 \\ - 4q^2 \rho_s^2 ((1-c)a_q - \mu_{\delta B}) \mu_{\delta B}. \end{aligned} \quad (72)$$

1. Weak-coupling limit

The weak-coupling limit is defined as

$$\frac{|\mu_{\delta B} - a_q|}{\mu} \ll 1, \quad (73)$$

because then the second term, i.e., coupling term, in the discriminant (72) is negligible compared to the first term. In the weak-coupling limit, expression (71) has different limiting expression, depending on the sign of $a_q + q^2 \rho_s^2 \mu_T - \mu - (1 - q^2 \rho_s^2) \mu$.

For $a_q + q^2 \rho_s^2 \mu_T - \mu - (1 - q^2 \rho_s^2) \mu_{\delta B} < 0$,

$$\gamma_q^+ \sim -q^2 \rho_s^2 (\mu_T + \mu_{\delta B}) + \frac{(\mu_{\delta B} - (1-c)a_q)r}{\mu^2} q^2 \rho_s^2 \mu, \quad (74)$$

$$\gamma_q^- \sim -\left(1 + \frac{\mu_{\delta B}}{\mu}\right) \mu + a_q - \frac{(\mu_{\delta B} - (1-c)a_q)r}{\mu^2} q^2 \rho_s^2 \mu. \quad (75)$$

For $a_q + q^2 \rho_s^2 \mu_T - \mu - (1 - q^2 \rho_s^2) \mu_{\delta B} > 0$, $a_q + q^2 \rho_s^2 \mu_T - \mu - (1 - q^2 \rho_s^2) \mu_{\delta B} > 0$,

$$\gamma_q^+ \sim a_q - \left(1 + \frac{\mu_{\delta B}}{\mu}\right) \mu + \frac{(\mu_{\delta B} - (1-c)a_q)^2}{\mu^2} q^2 \rho_s^2 \mu, \quad (76)$$

$$\gamma_q^- \sim -q^2 \rho_s^2 (\mu_T + \mu_{\delta B}) - \frac{(\mu_{\delta B} - (1-c)a_q)^2}{\mu^2} q^2 \rho_s^2 \mu. \quad (77)$$

It is interesting to compare these quasi-linear expressions to the linear expressions (38) and (39). The results for the first case are very similar to the linear expressions, with an additional stabilizing effect ($-q^2 \rho_s^2 \mu_T$) on the weakly-damped mode, due to particle flux modulation and a destabilization (a_q) of the strongly damped mode due to Reynolds stress modulation. The second case, however, is very different as in this case, it is the weakly-damped mode (the one with γ_q^+) that is destabilized by Reynolds stress modulation, and the strongly-damped mode (the one with γ_q^-) is further stabilized by particle flux modulation. Note, however, that since we consider a modulational instability, what matters is the spectrally-integrated growth rate, i.e., we need to sum over the wavenumbers q . Upon summation, the interplay between the dissipation rates and the turbulence intensity $|\phi_k|^2$ “hidden” in the terms a_q and μ_T solely determines the stability of the zonal modes.

III. ZONAL MODES—DRIFT WAVES PREDATOR-PREY MODEL

We now consider the non-linear dynamics of the interaction between the drift waves and the zonal modes.

A. Dynamics of zonal modes

In order to derive a predator-prey model, we only need two fields: turbulence ϕ_k and zonal potential $\delta\phi_q$, i.e., zonal flows, and we must close the dynamical feedback loop between primary drift waves and secondary zonal flows.

It would be desirable to solve numerically the set of three equations for the amplitude of turbulence ϕ_k , zonal flows $\delta\phi_q$, and zonal density δn_q , which could have chaotic states, but this is outside the scope of this paper, and left for future work. For simplicity, we consider the following ordering

$$\mu_{\delta B}, \mu_T \gg 1, \quad (78)$$

which means basically that the zonal density dynamics is slaved to the zonal potential dynamics. The zonal density response to zonal potential, obtained using Eq. (66) in the limit given by Eq. (78), is non-adiabatic

$$\delta n_q = \frac{\mu_{\delta B}}{\mu_T + \mu_{\delta B}} \delta\phi_q. \quad (79)$$

Replacing δn_q by expression (79), in the vorticity equation (67), we obtain

$$\begin{aligned} \frac{d}{dt} \delta\phi_q &= a_q \left(1 - (1-c) \frac{\mu_{\delta B}}{\mu_T + \mu_{\delta B}}\right) \delta\phi_q \\ &\quad - \mu_{\delta B} \left(1 - \frac{\mu_{\delta B}}{\mu_T + \mu_{\delta B}}\right) \delta\phi_q - \mu \delta\phi_q. \end{aligned} \quad (80)$$

Multiplying Eq. (80) by $\delta\phi_q^*$ and combining with the complex conjugate of Eq. (80) multiplied by $\delta\phi_q$, we obtain an equation describing the dynamics of zonal potential intensity

$$\begin{aligned} \frac{d|\delta\phi_q|^2}{dt} &= a_q \left(1 - (1-c) \frac{\mu_{\delta B}}{\mu_T + \mu_{\delta B}}\right) |\delta\phi_q|^2 \\ &\quad - \mu_{\delta B} \left(1 - \frac{\mu_{\delta B}}{\mu_T + \mu_{\delta B}}\right) |\delta\phi_q|^2 - \mu |\delta\phi_q|^2. \end{aligned} \quad (81)$$

Integrating Eq. (81) over the radial wavenumber k_x , multiplying by q^2 , and summing over q , we obtain an equation for the dynamics of zonal flow energy $E = \sum_q q^2 |\delta\phi_q|^2$

$$\frac{dE}{dt} = \alpha \epsilon E - \mu E - \frac{\mu_T \mu_{\delta B}}{\mu_T + \mu_{\delta B}} ((1 - \alpha') \alpha + 1) E. \quad (82)$$

B. Dynamics of turbulence energy

Due to wave action density conservation, the time variation of turbulence energy is linked to the correlation between turbulence energy and flow shear¹⁴

$$\frac{d\epsilon}{dt} = - \sum_{\mathbf{k}} v_g k_y \langle (\delta v'_{\mathbf{E} \times \mathbf{B}} + (1-c) \delta v'_{*e}) \tilde{N} \rangle. \quad (83)$$

Hence, we write the evolution of turbulence energy as

$$\frac{d\epsilon}{dt} = \gamma \epsilon - \int_{-\infty}^{+\infty} \sum_{\mathbf{k}} v_g k_y \langle (\delta v'_{\mathbf{E} \times \mathbf{B}} + (1-c) \delta v'_{*e}) \tilde{\epsilon} \rangle dk_x - \beta \epsilon^2. \quad (84)$$

The first term on the r.h.s of Eq. (84) models linear-drive. The second term comes from the k-space flux in the quasi-linear wave kinetic equation. It represents the effect of shearing, and the resulting refractive modulation of the drift wave spectrum, by the zonal $\mathbf{E} \times \mathbf{B}$ and electron diamagnetic flows. The last term accounts for non-linear damping, i.e., drift wave self-interaction. The second term on the r.h.s. of Eq. (84) can be calculated using the wave kinetic equation

$$\begin{aligned} \langle (\delta v'_{\mathbf{E} \times \mathbf{B}} + (1-c) \delta v'_{*e}) \tilde{N} \rangle &= k_y \sum_q q^2 |\delta\phi_q \\ &\quad - (1-c) \delta n_q|^2 R_q \frac{\partial \langle N \rangle}{\partial k_x}. \end{aligned} \quad (85)$$

After some algebra, Eqs. (84) and (85) give the prey equation

$$\frac{d\epsilon}{dt} = \gamma \epsilon - \left(1 - (1 - \alpha') \frac{\mu_{\delta B}}{\mu_T + \mu_{\delta B}}\right)^2 \alpha \epsilon E - \beta \epsilon^2, \quad (86)$$

with the following parameters

$$\alpha = \sum_q \sum_{\mathbf{k}} q^2 \tau_{ac} \frac{k_y^2}{(1 + k_{\perp}^2 \rho_s^2)^2}, \quad (87)$$

$$\alpha' = \sum_{\mathbf{k}} \frac{k_{\perp}^2 \rho_s^2}{1 + k_{\perp}^2 \rho_s^2}. \quad (88)$$

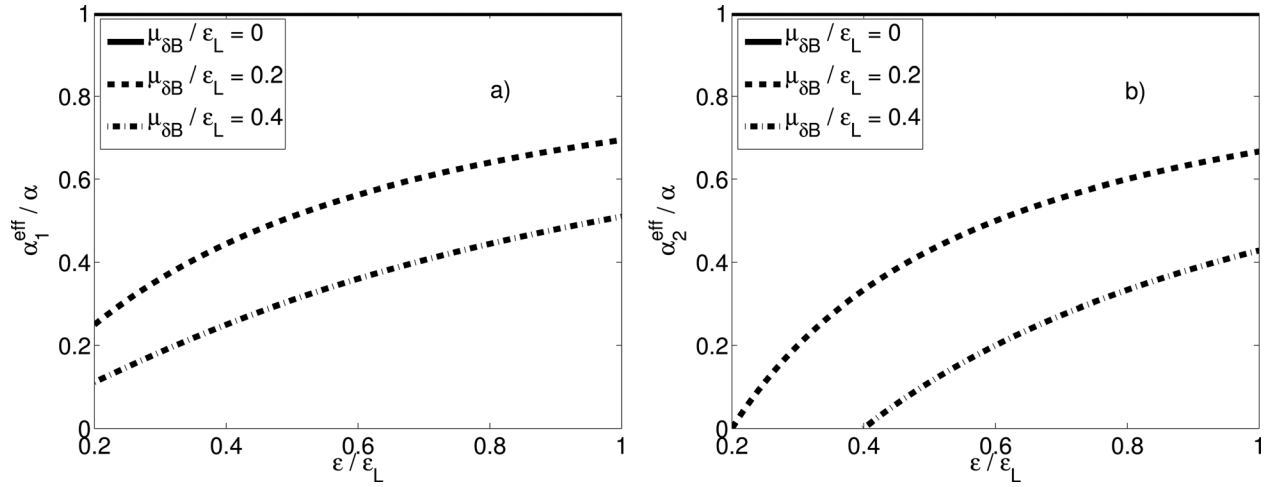


FIG. 2. Effective nonlinear coupling parameters vs. normalized turbulence energy $\frac{\epsilon}{\epsilon_L}$, for different values of the RMP coupling parameter: (a) $\frac{\alpha_1^{\text{eff}}}{\alpha}$ and (b) $\frac{\alpha_2^{\text{eff}}}{\alpha}$. The parameters are $\alpha = 1$, $\beta = 0.1$, $\gamma = 1$, $\mu = 2$, and $\alpha' = 0$.

C. Predator-prey model

We now assume that the parameter μ_T , proportional to the turbulent diffusivity D_T , takes the following form

$$\mu_T \sim \epsilon \quad (89)$$

This is valid in the adiabatic electron limit for the primary drift waves. Using assumption (89), the set of Eqs. (82) and (86) yield the following predator-prey model

$$\frac{d\epsilon}{dt} = \gamma\epsilon - \alpha_1^{\text{eff}}(\epsilon) - \beta\epsilon^2, \quad (90)$$

$$\frac{dE}{dt} = \alpha_2^{\text{eff}}(\epsilon) - \mu E, \quad (91)$$

where we define effective nonlinear coupling parameters

$$\alpha_1^{\text{eff}}(\epsilon) = \alpha \left((1 - \alpha') \frac{\mu_{\delta B}}{\epsilon + \mu_{\delta B}} - 1 \right)^2, \quad (92)$$

$$\alpha_2^{\text{eff}}(\epsilon) = \alpha - \frac{\mu_{\delta B}}{\epsilon + \mu_{\delta B}} ((1 - \alpha')\alpha + 1). \quad (93)$$

The effective nonlinear coupling parameters are plotted vs. turbulence energy, for different values of the (normalized) RMP coupling parameter $\frac{\mu_{\delta B}}{\epsilon_L}$ [Fig. 2]. Without RMPs ($\mu_{\delta B} = 0$), the two nonlinear coupling parameters coalesce into the parameter α of the standard predator-prey model, which ensures energy conservation between primary drift waves and secondary zonal flows.¹⁵ With RMPs, energy is *not* conserved due to the external magnetic energy from the RMP-producing coils. This is due to the intrinsically dissipative nature of the linear RMP coupling. The dissipative character of the nonlinearities arises from the slaving of the zonal density to the zonal potential. Close to the RMP Hmode threshold $\frac{\epsilon}{\epsilon_L} = 1$, the two coupling parameters are nearly equal, but they differ strongly far from threshold, i.e., for $\frac{\epsilon}{\epsilon_L} \ll 1$. Note that the $\alpha_2^{\text{eff}}(\epsilon)$ nonlinear coupling parameter is linked to the functional response F of predator-prey

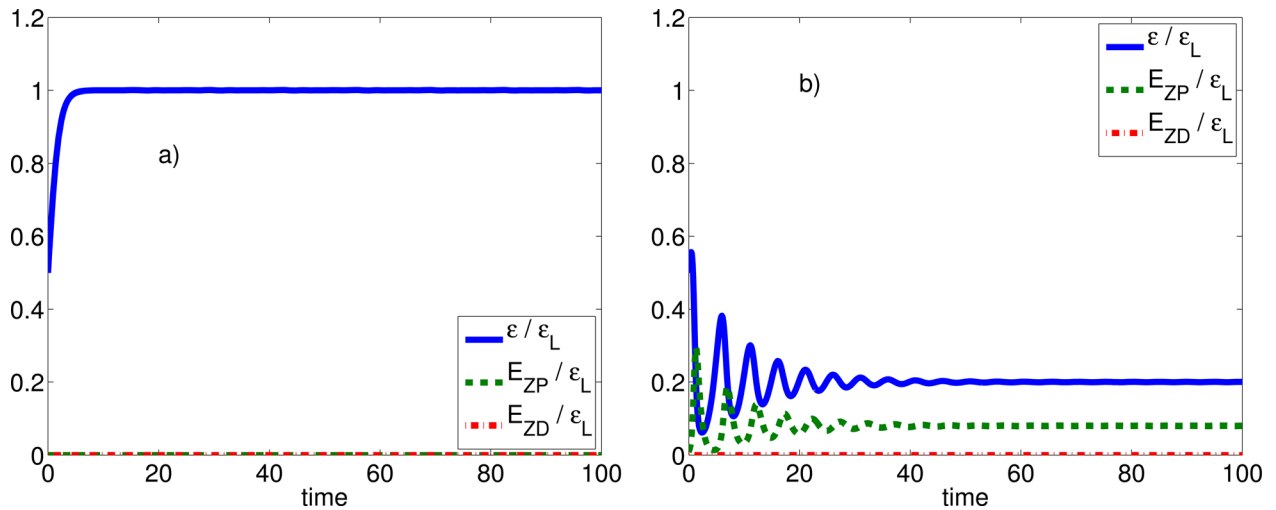


FIG. 3. (Color online) Dynamics of the model without RMPs ($\frac{\mu_{\delta B}}{\mu} = 0$): turbulence energy ϵ (solid line), and energies E_{ZP} , E_{ZD} associated to zonal flows (dashed line) and zonal density (dash-dotted line), for the two possible non-trivial states: (a) L mode-like state and (b) H mode like state. The parameters are the same as in Fig. 2.

models in ecology, i.e., $F = \alpha_2^{eff}(\epsilon)\epsilon$.^{16,17} More precisely, our model is characterized by a weakly nonlinear functional response, since the functional response derivative is

$$\frac{dF}{d\epsilon} = \alpha \left(1 - \frac{(1 - \alpha')\alpha + 1}{\alpha} \frac{\mu_{\delta B}}{\epsilon + \mu_{\delta B}} \right) \sim \alpha = \text{Cst.} \quad (94)$$

Moreover, in this model, the zonal density energy, obtained using expression (79), is a function of zonal flow energy and turbulence energy, i.e.,

$$E_{ZD} = \frac{\mu_{\delta B}^2}{(\epsilon + \mu_{\delta B})^2} E. \quad (95)$$

D. Results of the predator-prey model

The evolution and dynamics of the zonal modes—drift waves (ZM-DW) predator-prey model described by Eqs. (90) and (91), together with Eq. (95), are shown for different values of the RMP coupling parameter $\frac{\mu_{\delta B}}{\epsilon_L}$ [Figs. 4(a)–4(d)].

In the case of no RMPs, and zero initial zonal flow energy, an Lmode-like steady-state regime is reached, corresponding to no zonal flow and a high turbulence level [Fig. 3(a)]. In the case of no RMPs, but with a small initial

seed zonal flow, an H mode-like steady-state regime is reached, corresponding to the coexistence of ambient turbulence and zonal flows [Fig. 3(b)]. Accessing this state requires that the condition $\gamma > \frac{\beta}{\alpha}\mu$, be satisfied. As, $\gamma \sim \nabla p$, this is similar to a power threshold condition.

In the case with RMPs, a novel bifurcation occurs when the RMPs are turned on, e.g., above a critical coupling parameter $\frac{\mu_{\delta B}^1}{\epsilon_L} = 0$, after a transient period, a new steady-state is reached, where the level of *both* ambient turbulence and zonal flows increase with $\frac{\mu_{\delta B}}{\epsilon_L}$ [Figs. 4(b) and 4(c)]. However, above a critical value $\frac{\mu_{\delta B}^2}{\epsilon_L}$ of the RMP coupling parameter, a second bifurcation occurs: the energy of the ambient turbulence further increases with $\frac{\mu_{\delta B}}{\epsilon_L}$, but the energy of the zonal flows now decreases with $\frac{\mu_{\delta B}}{\epsilon_L}$. The dynamics is shown for $\frac{\mu_{\delta B}}{\mu} = 0.8$ [Fig. 4(d)]. The intermediate regime where the level of both ambient turbulence and zonal flows increases with $\frac{\mu_{\delta B}}{\epsilon_L}$ only appears below a certain value of the collisional drag μ . This unintuitive behavior may be linked to our reduction of the initial three-field problem (ϕ_k , $\delta\phi_q$, and δn_q), to a two-field problem (ϕ_k and $\delta\phi_q$), i.e., to the slaving of the zonal density dynamics to that of zonal potential. The

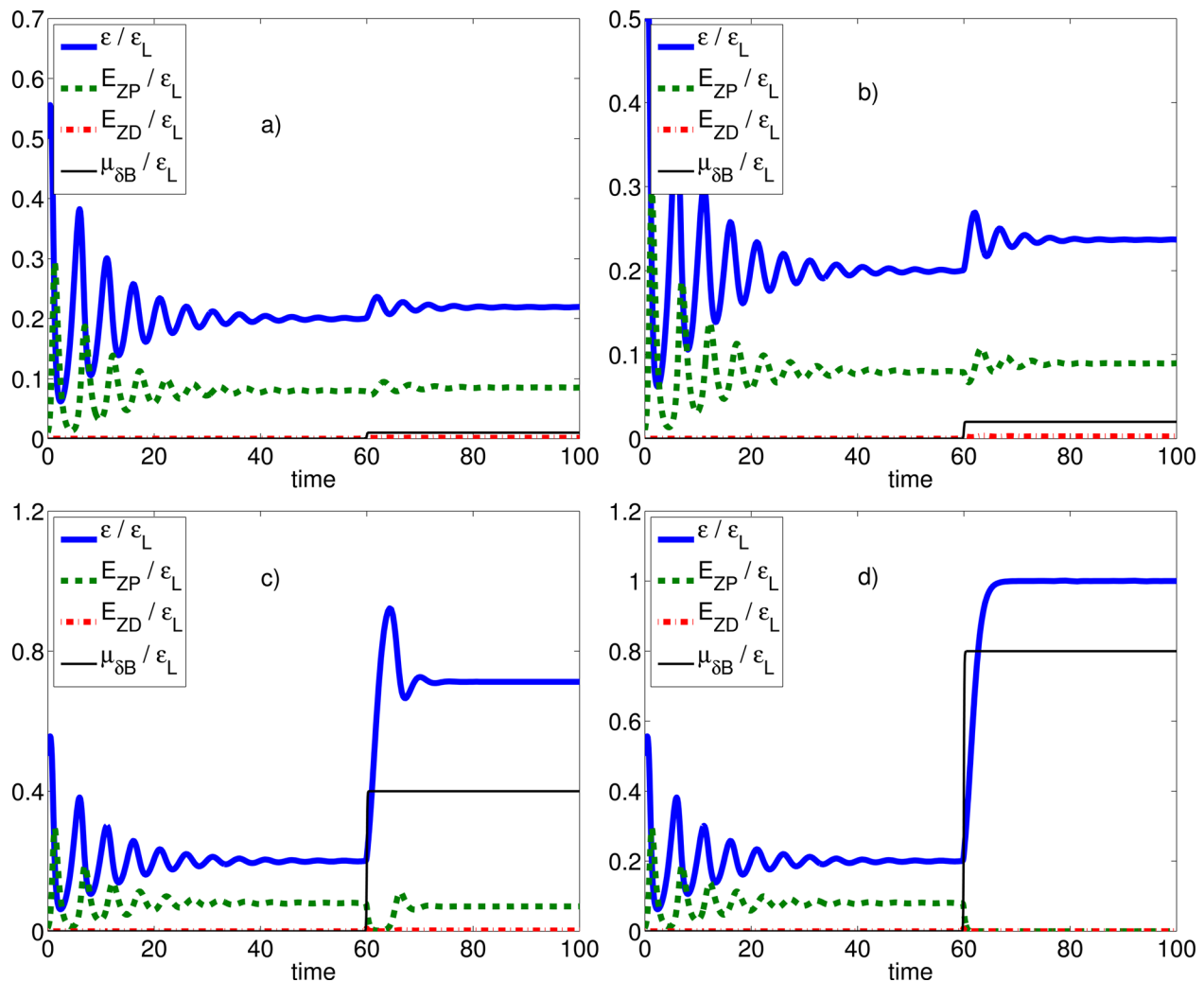


FIG. 4. (Color online) Dynamics of the zonal modes—drift waves predator-prey model: turbulence energy (solid line), and energies E_{ZP} , E_{ZD} associated to zonal flows (dashed line) and zonal density (dash-dotted line) before and during an RMP pulse applied at $t = 60$, for different values of the normalized coupling parameter $\frac{\mu_{\delta B}}{\epsilon_L}$: (a) for $\frac{\mu_{\delta B}}{\epsilon_L} = 0.01$, (b) for $\frac{\mu_{\delta B}}{\epsilon_L} = 0.2$, (c) for $\frac{\mu_{\delta B}}{\epsilon_L} = 0.4$, and (d) for $\frac{\mu_{\delta B}}{\epsilon_L} = 0.8$. The values of the parameters are: $\alpha = 1$, $\beta = 0.1$, $\gamma = 1$, $\mu = 2$, and $\alpha' = 0$.

TABLE II. Possible regimes for the predator-prey model Eqs. (90) and (91). The critical parameters are: $\frac{\mu_{\delta B}^2}{\epsilon_L} \simeq 0.14$ and $\frac{\mu_{\delta B}^3}{\epsilon_L} = \frac{2}{3}$, for the parameters of Fig. 2.

Without RMPs	H	$\mu_{\delta B} = 0$	$\epsilon_H E_{ZF} > 0$
Both	L	$\mu_{\delta B} = 0$ or $\mu_{\delta B} \geq \mu_{\delta B}^{c3}$	$\epsilon_L E_{ZF} = 0$
With RMPs	H^*	$\mu_{\delta B}^2 \leq \mu_{\delta B} < \mu_{\delta B}^{c3}$	$\epsilon_* \nearrow E_{ZF} \searrow$
	H^*	$0 < \mu_{\delta B} < \mu_{\delta B}^{c2}$	$\epsilon_* \nearrow E_{ZF} \nearrow$

dynamics of the full three-field problem is expected to have a wider set of possible states, including possible chaotic states. While the precise value of the critical coupling parameter $\frac{\mu_{\delta B}^2}{\epsilon_L}$ for the decay of zonal flows is difficult to predict, we estimate it numerically, for the parameters of Fig. (2), as: $\frac{\mu_{\delta B}^2}{\epsilon_L} \simeq 0.14$.

For a higher critical value $\frac{\mu_{\delta B}^3}{\epsilon_L}$ of the coupling parameter, a third bifurcation occurs at which the system reverts back to the Lmode-like state, characterized by no zonal flows and a high turbulence level. The critical coupling parameter can be evaluated using the fact that, at that bifurcation threshold, the energy of ambient turbulence reaches its maximum (ϵ_L), e.g., $\epsilon(\mu, \mu_{\delta B}^{c3}) = \epsilon_L = \frac{2}{\beta}$. For the parameters of Fig. 2, this yields $\frac{\mu_{\delta B}^3}{\epsilon_L} = \frac{2}{3}$. A summary of states is given [Table II]. Possible transitions between states are indicated schematically [Fig. 5].

E. Analysis of steady-state solutions

In order to understand RMP effects as predicted by the predator-prey model [Figs. 4(a)–4(d)], we study the steady-state solutions (i.e., fixed points) of the model. These are given by

$$\gamma\epsilon - \alpha_1^{eff}(\epsilon, \mu_{\delta B}) - \beta\epsilon^2 = 0, \quad (96)$$

$$\alpha_2^{eff}(\epsilon, \mu_{\delta B}) - \mu E = 0, \quad (97)$$

together with Eq. (95).

The first non-trivial solution of Eqs. (97) and (96) is an Lmode-like, no-flow state

$$\begin{pmatrix} \epsilon \\ E \end{pmatrix} = \begin{pmatrix} \epsilon_L \\ 0 \end{pmatrix}, \quad (98)$$

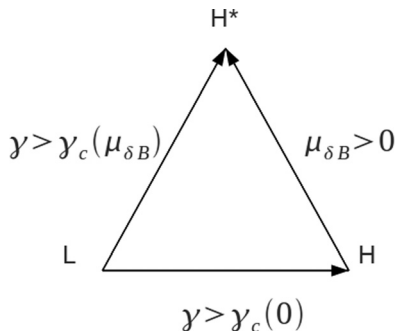


FIG. 5. Transition between states of the predator-prey model Eqs. (90) and (91).

with given by

$$\epsilon_L = \frac{\gamma}{\beta}. \quad (99)$$

The second non-trivial solution is a flow-dominated state, which we dub H^* (RMP Hmode), given by

$$\alpha_2^{eff}(\epsilon_{H^*})\epsilon_{H^*} - \mu = 0, \quad (100)$$

$$E_{H^*} = \beta \frac{\epsilon_L - \epsilon_{H^*}}{\alpha_1^{eff}(\epsilon_{H^*})}. \quad (101)$$

Note that, in order for E_{H^*} to remain positive and finite, expression (101) sets a constraint on the α_1^{eff} coupling parameter and a constraint on ϵ_{H^*} , namely: $\epsilon_{H^*} < \epsilon_L$. Similarly, since $\epsilon_{H^*} \geq 0$ and $\mu \geq 0$, expression (100) sets a constraint on the α_2^{eff} coupling parameter, namely: $\alpha_2^{eff} \geq 0$.

Equation (101) yields a quadratic equation with two solutions. However, one of them is negative and hence, not physical since kinetic energy is always positive. The unphysical solution is, therefore, discarded.

The energy of the physical solution, in normalized form, reads

$$\begin{aligned} \frac{\epsilon_{H^*}}{\epsilon_L} = \frac{1}{2\alpha} \left[(1 - \alpha'\alpha) \frac{\mu_{\delta B}}{\epsilon_L} + \frac{\epsilon_H}{\epsilon_L} \right] \\ + \frac{1}{2\alpha} \sqrt{\left[(1 - \alpha'\alpha) \frac{\mu_{\delta B}}{\epsilon_L} + \frac{\epsilon_H}{\epsilon_L} \right]^2 + 4 \frac{\mu_{\delta B}}{\epsilon_L} \frac{\epsilon_H}{\epsilon_L}}. \end{aligned} \quad (102)$$

The associated energy of the zonal flows is given by

$$\frac{E_{H^*}}{\epsilon_L} = \left((1 - \alpha') \frac{\frac{\mu_{\delta B}}{\epsilon_L}}{\frac{\epsilon_{H^*}}{\epsilon_L} + \frac{\mu_{\delta B}}{\epsilon_L}} - 1 \right)^{-2} \frac{\beta}{\alpha} \left(1 - \frac{\epsilon_{H^*}}{\epsilon_L} \right). \quad (103)$$

Without RMPs, e.g., $\mu_{\delta B} = 0$, we recover the Hmode-like state of the standard ZF-DW predator-prey model

$$\begin{pmatrix} \epsilon_{H^*} \\ E_{H^*} \end{pmatrix} = \begin{pmatrix} \epsilon_H \\ E_H \end{pmatrix}, \quad \text{for } \mu_{\delta B} = 0, \quad (104)$$

with the turbulence energy ϵ_H and zonal flow energy E_H given by

$$\frac{\epsilon_H}{\epsilon_L} = \frac{\mu}{\alpha\epsilon_L}, \quad (105)$$

$$\frac{E_H}{\epsilon_L} = \frac{\beta}{\alpha} \left(1 - \frac{\epsilon_H}{\epsilon_L} \right). \quad (106)$$

At fixed collisionality, i.e., $\mu = \mu(\nu^*)$ constant, the zonal flow energy and associated ambient turbulence energy have a nonlinear dependence on the RMP coupling parameter $\frac{\mu_{\delta B}}{\epsilon_L}$ [Fig. 6]. In particular, zonal flow energy is maximal for a critical value of the RMP coupling parameter $\frac{\mu_{\delta B}}{\epsilon_L} > \frac{\mu_{\delta B}^2}{\epsilon_L}$. The critical RMP coupling parameter $\frac{\mu_{\delta B}^2}{\epsilon_L}$ can be calculated by considering that, at the bifurcation, the following condition is satisfied:

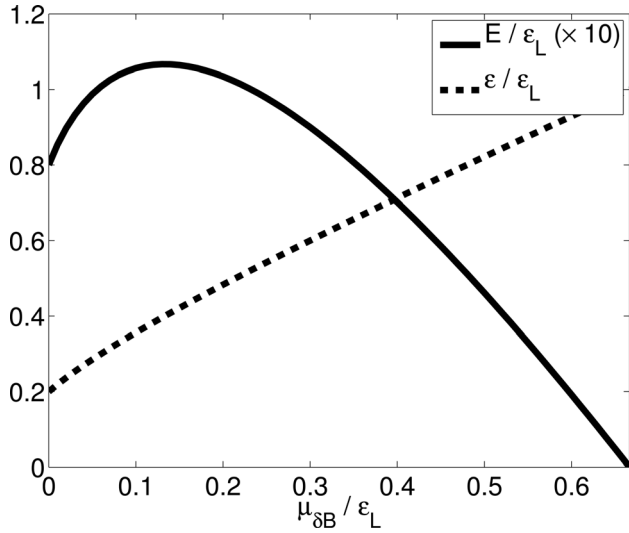


FIG. 6. Zonal flow energy and ambient turbulence energy vs. the normalized RMP coupling parameter. Parameters are the same as in Fig. 4.

$$\left. \frac{\partial E_{H^*}}{\partial \mu_{\delta B}} \right|_{\mu_{\delta B}^c} = 0. \quad (107)$$

This expression is most easily evaluated numerically. For the parameters of Fig. 7, its value is approximately $\frac{\mu_{\delta B}^c}{\epsilon_L} \simeq 0.14$.

In the strong-RMP limit $\frac{\mu_{\delta B}}{\epsilon_L} \gg \frac{\epsilon_H}{\epsilon_L}$, expression (103) reduces to

$$\frac{\epsilon_{H^*}}{\epsilon_L} \sim \left(\frac{1}{\alpha} - \alpha' \right) \frac{\mu_{\delta B}}{\epsilon_L} + (\alpha + 1) \frac{\epsilon_H}{\epsilon_L}. \quad (108)$$

However, as is clear from the numerical results [Figs. 4(a)–4(d)], this expression is only valid below a critical value $\frac{\mu_{\delta B}^c}{\epsilon_L}$ of the coupling parameter, which we will see, corresponds to a power threshold. Physically, the H^* mode can only be accessed for $\frac{\epsilon_{H^*}}{\epsilon_L} < 1$, i.e., $\gamma > \gamma_c = \beta \epsilon_{H^*}$ which is equivalent to a power threshold. Interestingly, in the H^* mode, the power threshold is a function of the RMP coupling parameter: $\gamma_c = \gamma_c(\mu_{\delta B})$. The dependence of the power threshold on

$\mu_{\delta B}$, expressed in normalized form $\frac{\Delta \gamma_c}{\gamma_c}$, is shown for different values of the collisional drag μ [Fig. 8]. Hence, the critical parameter $\frac{\mu_{\delta B}^c}{\epsilon_L}$ is given by the following equation:

$$\alpha_2^{eff}(\epsilon_L, \mu_{\delta B}^c) \epsilon_L - \mu = 0. \quad (109)$$

The critical parameter $\frac{\mu_{\delta B}^c}{\epsilon_L}$ reads

$$\frac{\mu_{\delta B}^c}{\epsilon_L} = \frac{\alpha - \frac{\mu}{\epsilon_L}}{1 + \frac{\mu}{\epsilon_L}}. \quad (110)$$

The energy of zonal flows E and the associated turbulence energy ϵ of the RMP Hmode are plotted as a function of the parameters $\frac{\nu^*}{\epsilon_L}$ and $\frac{\mu_{\delta B}}{\epsilon_L}$, for a value $\alpha = 1$ of the α parameter [Fig. 7]. Both energies are normalized to the ambient turbulence energy of the Lmode-like state $\epsilon_L = \gamma/\beta$.

IV. DISCUSSION AND CONCLUSIONS

The results of the analysis of the drift wave—zonal mode predator-prey model, derived from a generalization of the Hasegawa-Wakatani equations to include RMPs, recover the damping of zonal flows observed in experiments.⁸ We identify a new state, which we call the RMP Hmode (H^*). Without RMPs, the possible states of the system are an Lmode-like state with no zonal flows and high turbulence and an Hmode-like state (accessible above a power threshold) with zonal flows and a low turbulence level. With RMPs, the possible states are the Lmode-like state and the novel H^* mode (accessible above an RMP amplitude-dependent power threshold) with either enhanced or damped zonal flows, depending on RMP amplitude, and a low turbulence level. The H^* mode is similar to the Hmode-like state of the standard predator-prey model, but characterized by a nonlinear dependence of the power threshold on the RMP coupling parameter $\mu_{\delta B}$. More precisely, the RMP Hmode threshold increases with $\mu_{\delta B} \sim \left(\frac{\delta B_L}{B} \right)^2$. Note, however, that to obtain this scaling, we

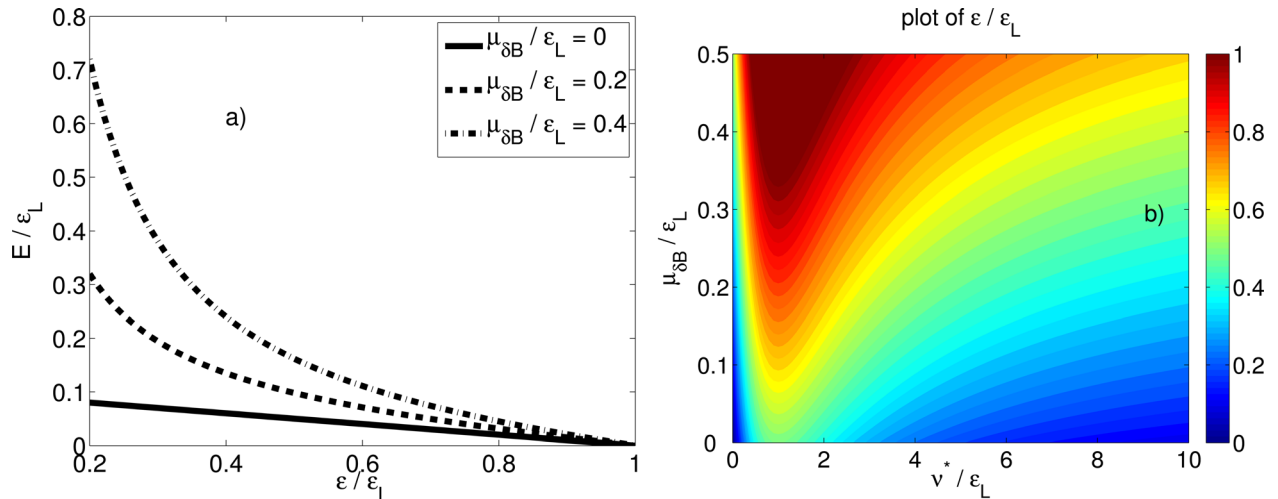


FIG. 7. (Color online) Steady-state solutions of the ZM-DW predator prey model. (a) energy of zonal flows $\frac{E}{\epsilon_L}$ vs. normalized turbulence energy $\frac{\epsilon}{\epsilon_L}$ for different values of the normalized RMP coupling parameter $\frac{\mu_{\delta B}}{\epsilon_L}$ and (b) associated normalized turbulence energy $\frac{\epsilon}{\epsilon_L}$ vs. normalized coupling parameter $\frac{\mu_{\delta B}}{\epsilon_L}$ and normalized collisionality $\frac{\nu^*}{\epsilon_L}$. Here, the value of the parameter α is $\alpha = 1$.

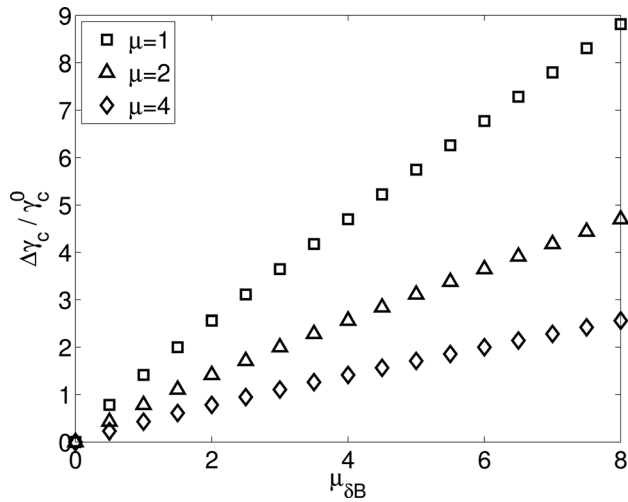


FIG. 8. RMPs increase the power threshold: relative variation of power threshold $\frac{\Delta\gamma_c}{\gamma_c^0}$ vs. RMP coupling parameter $\mu_{\delta B}$, for different values of the collisional drag μ .

assumed that the particle turbulent diffusivity is independent of the linear drive γ . If, instead, we take the particle turbulent diffusivity to be proportional to linear drive, e.g., $D_T \sim \gamma \rho_s^2 \epsilon$, this yields a timescale for the particle turbulent diffusion process and hence, for the zonal density damping, namely γ^{-1} . Moreover, with this relation, the turbulence level of the RMP Hmode now depends explicitly on the linear drive γ , and a simple calculation shows that the RMP power threshold is now determined by a cubic equation with a $(\frac{\delta B_r}{B})^2$ scaling in the weak-RMP limit, but a $(\frac{\delta B_r}{B})^{2/3}$ scaling in the strong-RMP limit. An increase of the H-mode power threshold with RMP strength has been observed in recent experiments.⁵ Moreover, we find that the RMP Hmode threshold is very sensitive to collisionality ν^* . This may be related to the observation that RMPs are more efficient at mitigating ELMs for low collisionality.^{2,5} However, experiments show that the resonant character of RMPs, e.g., even or odd parity of the coils, determines at which collisionality RMPs are effective.⁵ Since our model does not distinguish between RMPs that are in even or odd parity, we cannot address this issue here. We stress in our model that damping and/or suppression of zonal flows is found only for certain regions of parameter space, e.g., for the strong coupling limit $\frac{\mu_{\delta B}}{\epsilon_L} \gg \frac{\mu_{\delta B}^2}{\epsilon_L}$, which corresponds to the strong-RMP limit. In the weak-coupling limit $\frac{\mu_{\delta B}}{\epsilon_L} \ll \frac{\mu_{\delta B}^2}{\epsilon_L}$, our predator-prey model suggests that zonal flows are instead enhanced by the RMPs. We stress, though, that fluctuation levels are predicted to *increase* for RMP switch-on in both the weak and strong RMP regimes.

V. CONCLUSION

In this work, we studied the effects of RMPs on zonal flows and associated zonal density modulations, using an extended Hasegawa-Wakatani model. In physical terms, RMPs enable the radial diffusion of electrons parallel to perturbed magnetic surfaces, but perpendicular to unperturbed ones, a process known as magnetic flutter. This process can compete with the cross-field transport of polarization charge

which is the agent of guiding-center ambipolarity breaking responsible for zonal flow formation. This simple model shows that, in presence of RMPs, the usual drift-wave zonal-flow paradigm is no longer strictly valid. With RMPs, the zonal potential (i.e., secondary zonal flows), in addition to being indirectly (i.e., nonlinearly) coupled to primary drift waves, are also directly (i.e., *linearly*) coupled to secondary zonal density perturbations. The main resulting effect is that, through this direct linear coupling, the zonal flows are damped by the turbulent particle diffusivity.

In order to quantify the damping of zonal flows, we derived a predator-prey model based on the extended Hasegawa-Wakatani model, where we approximated that the zonal density is slaved to the zonal potential, and we also considered the evolution of primary drift wave energy, in order to close the feedback-loop. The dynamics of this predator-prey model exhibits a rich variety of behaviour, depending on the value of the control parameter $\mu_{\delta B}$, where $\mu_{\delta B} = \frac{D_{\parallel}}{\rho_s^2 \gamma_{ZF}} [\frac{\delta B_r}{B}]^2$. For $\mu_{\delta B} = 0$, the system is bistable, being either in a Lmode-like regime, characterized by no zonal flow $E_L = 0$ and a high turbulence level, or in a Hmode-like regime, characterized by a finite level of zonal flows $E_H > 0$, and a low turbulence level $\epsilon_H < \epsilon_L$. The Hmode-like regime is accessible only above a critical value $\gamma > \gamma_c$ of the linear drive, i.e., above a power threshold.

For $\mu_{\delta B} > 0$, the system bifurcates to a new regime, which we call the RMP Hmode (H^*). This regime bears some similarity with the Hmode-like regime, but has two major differences: (i) the threshold increases with the control parameter $\mu_{\delta B}$, e.g., $\gamma_c = \gamma_c(\mu_{\delta B})$ and (ii) the zonal flow energy can increase or decrease with the control parameter $\mu_{\delta B}$, depending on the value of $\mu_{\delta B}$. For $\mu_{\delta B}^{c1} < \mu_{\delta B} < \mu_{\delta B}^{c2}$, both the zonal flow energy and ambient turbulence energy increase with $\mu_{\delta B}$. Here, $\mu_{\delta B}^{c2}$ denotes the threshold for the onset of the H^* regime, and $\mu_{\delta B}^{c2} = \mu_{\delta B}^{c2}(\nu^*)$ is a function of collisionality ν^* . For $\mu_{\delta B}^{c2} \leq \mu_{\delta B} < \mu_{\delta B}^{c3}$, the zonal flow energy decreases with $\mu_{\delta B}$ while the turbulence energy keeps increasing. The threshold $\mu_{\delta B}^{c3} = \mu_{\delta B}^{c3}(\nu^*)$ depends on collisionality. In order to test these predictions, future experiments of the form of Ref. 18 would be of a great interest.

ACKNOWLEDGMENTS

The authors would like to thank Y. Xu, G. Dif-Pradalier, P. Beyer, G. McKee, K. Ida, and P. Manz for useful discussions. This work was supported by the World Class Institute (WCI) Program of the National Research Foundation of Korea (NRF) funded by the Ministry of Education, Science and Technology of Korea (MEST).

APPENDIX: ANALYSIS OF NEW STEADY-STATE AND INTERMEDIATE CALCULATIONS

1. Stability analysis of the RMP Hmode

In order to simplify the stability analysis of the RMP Hmode state H^* , we consider the limit $\alpha' = 0$. In this case, the predator-prey equations read

$$\frac{d\epsilon}{dt} = \gamma\epsilon - \beta\epsilon^2 - \hat{\alpha}_1^{\text{eff}}(\epsilon), \quad (\text{A1})$$

$$\frac{dE}{dt} = \hat{\alpha}_2^{\text{eff}}(\epsilon) - \mu E, \quad (\text{A2})$$

with the coupling parameters, for $\alpha' = 0$, given by

$$\hat{\alpha}_1^{\text{eff}}(\epsilon) = \frac{\epsilon^2}{(\epsilon + \mu_{\delta B})^2} \alpha, \quad (\text{A3})$$

$$\hat{\alpha}_2^{\text{eff}}(\epsilon) = \frac{\epsilon - \frac{1}{\alpha} \mu_{\delta B}}{\epsilon + \mu_{\delta B}} \alpha. \quad (\text{A4})$$

The Jacobian matrix is

$$J(\epsilon, E) = \begin{pmatrix} \gamma - 2\beta\epsilon - \left[\frac{d \ln \hat{\alpha}_1^{\text{eff}}}{d\epsilon} + 1 \right] \hat{\alpha}_1^{\text{eff}}(\epsilon) E & -\hat{\alpha}_1^{\text{eff}}(\epsilon) \epsilon \\ \left[\frac{d \ln \hat{\alpha}_2^{\text{eff}}}{d\epsilon} + 1 \right] \hat{\alpha}_2^{\text{eff}}(\epsilon) E & \hat{\alpha}_2^{\text{eff}}(\epsilon) \epsilon - \mu \end{pmatrix}, \quad (\text{A5})$$

where the logarithmic derivatives are

$$\frac{d \ln \hat{\alpha}_1^{\text{eff}}}{d\epsilon} = \frac{2\mu_{\delta B}}{\epsilon + \mu_{\delta B}}, \quad (\text{A6})$$

$$\frac{d \ln \hat{\alpha}_2^{\text{eff}}}{d\epsilon} = \frac{\alpha + 1}{\alpha} \frac{\mu_{\delta B} \epsilon}{(\epsilon + \mu_{\delta B})(\epsilon - \mu_{\delta B}/\alpha)}. \quad (\text{A7})$$

In the weak-RMP limit, $\frac{\mu_{\delta B}}{\epsilon} \ll 1$, keeping only terms first-order in $\frac{\mu_{\delta B}}{\epsilon}$, the coupling parameters and their logarithmic derivatives reduce to

$$\hat{\alpha}_1^{\text{eff}}(\epsilon) \sim \left(1 - 2 \frac{\mu_{\delta B}}{\epsilon} \right) \alpha, \quad (\text{A8})$$

$$\frac{d \ln \hat{\alpha}_1^{\text{eff}}}{d\epsilon} \sim 2 \frac{\mu_{\delta B}}{\epsilon}, \quad (\text{A9})$$

$$\hat{\alpha}_2^{\text{eff}}(\epsilon) \sim \left(1 - \frac{\alpha + 1}{\alpha} \frac{\mu_{\delta B}}{\epsilon} \right) \alpha, \quad (\text{A10})$$

$$\frac{d \ln \hat{\alpha}_2^{\text{eff}}}{d\epsilon} = \frac{\alpha + 1}{\alpha} \frac{\mu_{\delta B}}{\epsilon}. \quad (\text{A11})$$

Using these approximations, the Jacobian (A6) reduces to

$$J(\epsilon, E) \sim \begin{pmatrix} \gamma - 2\beta\epsilon - \alpha E & -\left(1 - 2 \frac{\mu_{\delta B}}{\epsilon} \right) \alpha \epsilon \\ \alpha E & \left(1 - \frac{\alpha + 1}{\alpha} \frac{\mu_{\delta B}}{\epsilon} \right) \alpha \epsilon - \mu \end{pmatrix}. \quad (\text{A12})$$

This is equivalent to

$$J(\epsilon, E) \sim \begin{pmatrix} \gamma - 2\beta\epsilon - \alpha E & -\alpha\epsilon + 2\alpha\mu_{\delta B} \\ \alpha E & \alpha\epsilon - (\alpha + 1)\mu_{\delta B} - \mu \end{pmatrix}. \quad (\text{A13})$$

Now we consider the steady-state H^* . In the weak-RMP limit it is given by

$$\begin{aligned} \epsilon_* &\sim \frac{\mu}{2\alpha} \left(1 + \frac{\mu_{\delta B}}{\mu} \right) + \frac{\mu}{2\alpha} \sqrt{\left(1 + 2 \frac{\mu_{\delta B}}{\mu} \right) + 4\alpha \frac{\mu_{\delta B}}{\mu}} \\ &\sim \left(1 + (\alpha + 1) \frac{\mu_{\delta B}}{\mu} \right) \frac{\mu}{\alpha}, \end{aligned} \quad (\text{A14})$$

$$E_{H^*} \sim \frac{\gamma - \beta\epsilon_*}{\alpha}. \quad (\text{A15})$$

Plugging these expressions in (A13), we get

$$J(\epsilon_*, E_{H^*}) \sim \begin{pmatrix} -\left(1 + (\alpha + 1) \frac{\mu_{\delta B}}{\mu} \right) \frac{\beta\mu}{\alpha} & -\left(1 - (\alpha - 1) \frac{\mu_{\delta B}}{\mu} \right) \mu \\ \gamma - \left(1 + (\alpha + 1) \frac{\mu_{\delta B}}{\mu} \right) \frac{\beta\mu}{\alpha} & 0 \end{pmatrix}. \quad (\text{A16})$$

The eigenvalues λ of the Jacobian matrix (A16) are given by

$$\begin{aligned} \lambda^2 + \left(1 + (\alpha + 1) \frac{\mu_{\delta B}}{\mu} \right) \frac{\beta\mu}{\alpha} \lambda \\ + \left(1 - (\alpha - 1) \frac{\mu_{\delta B}}{\mu} \right) \left[\gamma - \left(1 + (\alpha + 1) \frac{\mu_{\delta B}}{\mu} \right) \frac{\beta\mu}{\alpha} \right] \mu. \end{aligned} \quad (\text{A17})$$

The discriminant of Eq. (A17) is

$$\begin{aligned} \Delta = \left(1 + (\alpha + 1) \frac{\mu_{\delta B}}{\mu} \right)^2 \frac{\beta^2 \mu^2}{\alpha^2} \\ - 4 \left(1 - (\alpha - 1) \frac{\mu_{\delta B}}{\mu} \right) \left[\gamma - \left(1 + (\alpha + 1) \frac{\mu_{\delta B}}{\mu} \right) \frac{\beta\mu}{\alpha} \right] \mu. \end{aligned} \quad (\text{A18})$$

Since the H^* mode is accessible only above a threshold $\gamma > \frac{\beta\mu}{\alpha}$, the discriminant (A18) is strictly negative: $\Delta < 0$, and the eigenvalues are hence complex. The eigenvalues are thus

$$\lambda = \sigma \pm i\omega, \quad (\text{A19})$$

with

$$\sigma = -\left(1 + (\alpha + 1) \frac{\mu_{\delta B}}{\mu} \right) \frac{\beta\mu}{2\alpha} < 0, \quad (\text{A20})$$

$$\omega = \frac{1}{2} \sqrt{|\Delta|}. \quad (\text{A21})$$

Since $\text{Re}\lambda = \sigma < 0$, the H^* mode is thus a hyperbolic, attractor fixed-point. Moreover, Eq. (A18) yields the threshold of the H^* mode, in the weak-RMP limit, namely

$$\gamma_c^{H^*}(\mu_{\delta B}) \sim \gamma_c^H + \frac{\beta(\alpha + 1)}{\alpha} \mu_{\delta B} \quad \text{for} \quad \frac{\mu_{\delta B}}{\mu} \ll 1, \quad (\text{A22})$$

where $\gamma_c^H = \frac{\beta\mu}{\alpha}$ denotes the H -mode threshold.

2. Derivation of Eqs. (12) and (13)

The surface average of the first term on the r.h.s. of Eqs. (9) and (10) vanishes, and we get

$$\begin{aligned} \frac{\partial}{\partial t} \langle n \rangle + \frac{\partial}{\partial x} \langle \tilde{v}_x \tilde{n} \rangle &= D_{\parallel} \left\langle \tilde{B}_x \frac{\partial}{\partial x} (ik_{\parallel 0} (\tilde{n} - \tilde{\phi})) \right\rangle \\ &+ D_{\parallel} \left\langle \tilde{B}_x \frac{\partial}{\partial x} \left(\tilde{B}_x \frac{\partial}{\partial x} (n - \phi) \right) \right\rangle, \end{aligned} \quad (\text{A23})$$

$$\begin{aligned} \rho_s^2 \frac{\partial}{\partial t} \nabla_{\perp}^2 \langle \phi \rangle + \mu \rho_s^2 \nabla_{\perp}^2 \langle \phi \rangle + \rho_s^2 \frac{\partial}{\partial x} \langle \tilde{v}_x \nabla_{\perp}^2 \tilde{\phi} \rangle \\ = D_{\parallel} \langle \tilde{B}_x \frac{\partial}{\partial x} (ik_{\parallel 0} (\tilde{n} - \tilde{\phi})) \rangle + D_{\parallel} \langle \tilde{B}_x \frac{\partial}{\partial x} \left(\tilde{B}_x \frac{\partial}{\partial x} (n - \phi) \right) \rangle, \end{aligned} \quad (\text{A24})$$

where $\tilde{B}_x = -ik_y \tilde{\psi}$ (normalized to B_0) is the magnetic field radial perturbation.

Replacing \tilde{B}_x by its expression, we have

$$\begin{aligned} \frac{\partial}{\partial t} \langle n \rangle + \frac{\partial}{\partial x} \langle \tilde{v}_x \tilde{n} \rangle &= -D_{\parallel} \left\langle k_y^2 \tilde{\psi} \frac{\partial}{\partial x} \left(\frac{x - x_{k_y}}{L_s} (\tilde{n} - \tilde{\phi}) \right) \right\rangle \\ &+ D_{\parallel} \left\langle k_y^2 \tilde{\psi} \frac{\partial}{\partial x} \left(\tilde{\psi} \frac{\partial}{\partial x} (n - \phi) \right) \right\rangle, \end{aligned} \quad (\text{A25})$$

$$\begin{aligned} \rho_s^2 \frac{\partial}{\partial t} \nabla_{\perp}^2 \langle \phi \rangle + \mu \rho_s^2 \nabla_{\perp}^2 \langle \phi \rangle + \rho_s^2 \frac{\partial}{\partial x} \langle \tilde{v}_x \nabla_{\perp}^2 \tilde{\phi} \rangle \\ = -D_{\parallel} \left\langle k_y^2 \tilde{\psi} \frac{\partial}{\partial x} \left(\frac{x - x_{k_y}}{L_s} (\tilde{n} - \tilde{\phi}) \right) \right\rangle \\ + D_{\parallel} \left\langle k_y^2 \tilde{\psi} \frac{\partial}{\partial x} \left(\tilde{\psi} \frac{\partial}{\partial x} (n - \phi) \right) \right\rangle. \end{aligned} \quad (\text{A26})$$

3. Derivation of Eqs. (59) and (60)

The evolution of potential enstrophy density reads

$$\begin{aligned} \frac{d}{dt} \delta \Omega + iq v_g \delta \Omega + |\gamma_k| \delta \Omega \\ = k_y q^2 \left(\frac{\delta n_q}{1 + k_{\perp}^2 \rho_s^2} - \delta \phi_q \right) \frac{\partial}{\partial k_x} \langle \Omega \rangle. \end{aligned} \quad (\text{A27})$$

Since we consider zero-frequency modulations ($d(\delta \Omega)/dt = 0$), this yields

$$\delta \Omega = \frac{q^2 k_y}{iq v_g + |\gamma_k|} \left(\delta \phi_q - \frac{\delta n_q}{1 + k_{\perp}^2 \rho_s^2} \right) \frac{\partial}{\partial k_x} \langle \Omega \rangle. \quad (\text{A28})$$

4. Simplification of the discriminant of Eq. (71)

The discriminant Δ in Eq. (71) has the form

$$\begin{aligned} \Delta &= (a_q - (\mu + \mu_{\delta B}) - q^2 \rho_s^2 (\mu_T + \mu_{\delta B}))^2, \quad (\text{A29}) \\ &+ 4q^2 \rho_s^2 [(a_q - (\mu + \mu_{\delta B})) \mu_T - \mu_{\delta B} (\mu - ca_q)]. \end{aligned} \quad (\text{A30})$$

Rearranging terms, we get

$$\begin{aligned} \Delta &= (a_q - (\mu + \mu_{\delta B}) - q^2 \rho_s^2 (\mu_T + \mu_{\delta B}))^2 \\ &+ 4q^2 \rho_s^2 [(a_q - (\mu + \mu_{\delta B})) (\mu_T + \mu_{\delta B}) \\ &- \mu_{\delta B} (\mu - ca_q)] - 4q^2 \rho_s^2 (a_q - (\mu + \mu_{\delta B})) \mu_{\delta B}, \end{aligned} \quad (\text{A31})$$

and we obtain expression (72) given in the main text.

¹T. E. Evans, R. A. Moyer, P. R. Thomas, J. G. Watkins, T. H. Osborne, J. A. Boedo, E. J. Doyle, M. E. Fenstermacher, K. H. Finken, R. J. Groebner, M. Groth, J. H. Harris, R. J. La Haye, C. J. Lasnier, S. Masuzaki, N. Ohya, D. G. Pretty, T. L. Rhodes, H. Reimerdes, D. L. Rudakov, M. J. Schaffer, G. Wang, and L. Zeng, *Phys. Rev. Lett.* **92**, 235003 (2004).

²K. H. Burrell, T. E. Evans, E. J. Doyle, M. E. Fenstermacher, R. J. Groebner, A. W. Leonard, R. A. Moyer, T. H. Osborne, M. J. Schaffer, P. B. Snyder, P. R. Thomas, W. P. West, J. A. Boedo, A. M. Garofalo, P. Gohil, G. L. Jackson, R. J. La Haye, C. J. Lasnier, H. Reimerdes, T. L. Rhodes, J. T. Scoville, W. M. Solomon, D. M. Thomas, G. Wang, J. G. Watkins, and L. Zeng, *Plasma Phys. Controlled Fusion* **47**, B37 (2005).

³K. H. Finken, B. Unterberg, Y. Xu, S. S. Abdullaev, M. Jakubowski, M. Lehnen, M. F. M. de Bock, S. Bozhenkov, S. Brezinsek, C. Busch, I. G. J. Classen, J. W. Coenen, D. Harting, M. von Hellermann, S. Jachmich, R. J. E. Jaspers, Y. Kikuchi, A. Kramer-Flecken, Y. Liang, M. Mitri, P. Peleman, A. Pospieszczyk, D. Reiser, D. Reiter, U. Samm, D. Schega, O. Schmitz, S. Soldatov, M. Van Schoor, M. Vergote, R. R. Weynants, R. Wolf, O. Zimmermann, and the TEXTOR Team, *Nucl. Fusion* **47**, 522 (2007).

⁴Y. Liang, H. R. Koslowski, P. R. Thomas, E. Nardon, S. Jachmich, A. Alfier, G. Arnoux, Y. Baranov, M. Becoulet, M. Beurskens, R. Coelho, Th. Eich, E. De La Luna, W. Fundamenski, S. Gerasimov, C. Giroud, M. P. Gryaznevich, D. Harting, A. Huber, A. Kreter, L. Moreira, V. Parail, S. D. Pinches, S. Saarelma, O. Schmitz, and JET-EFDA contributors, *Nucl. Fusion* **50**, 025013 (2010).

⁵A. Kirk, Y. Liu, E. Nardon, P. Tamain, P. Cahyna, I. Chapman, P. Denner, H. Meyer, S. Mordijck, D. Temple, and the MAST team, *Plasma Phys. Controlled Fusion* **53**, 065011 (2011).

⁶M. Leconte, P. Beyer, X. Garbet, and S. Benkadda, *Nucl. Fusion* **50**, 054008 (2010).

⁷P. Beyer, F. de Solminihac, M. Leconte, X. Garbet, F. L. Waelbroeck, A. I. Smolyakov, and S. Benkadda, *Plasma Phys. Controlled Fusion* **53**, 054003 (2011).

⁸Y. Xu, D. Carralero, C. Hidalgo, S. Jachmich, P. Manz, E. Martinez, B. van Milligen, M. A. Pedrosa, M. Ramisch, I. Shesterikov, C. Silva, M. Spolaore, U. Stroth, and N. Vianello, *Nucl. Fusion* **51**, 063020 (2011).

⁹P. Beyer, X. Garbet, S. Benkadda, P. Ghendrih, and Y. Sarazin, *Plasma Phys. Controlled Fusion* **44**, 2167 (2002).

¹⁰P. H. Diamond, S.-I. Itoh, K. Itoh, and T. S. Hahm, *Plasma Phys. Controlled Fusion* **47**, R35 (2005).

¹¹P. Manz, M. Ramisch, and U. Stroth, *Phys. Plasmas* **16**, 042309 (2009).

¹²P. H. Diamond, M. N. Rosenbluth, F. L. Hinton, M. Malkov, J. Fleischer, and A. Smolyakov, *17th IAEA Fusion Energy Conference, IAEA-CN-69/TH3/1* (International Atomic Energy Agency, Vienna, 1998).

¹³A. I. Smolyakov, P. H. Diamond, and V. I. Shevchenko, *Phys. Plasmas* **7**, 1349 (2000).

¹⁴P. H. Diamond, M. N. Rosenbluth, E. Sanchez, C. Hidalgo, B. Van Milligen, T. Estrada, B. Branas, M. Hirsch, H. J. Hartfuss, and B. A. Carreras, *Phys. Rev. Lett.* **84**, 4842 (2000).

¹⁵P. H. Diamond, Y.-M. Liang, B. A. Carreras, and P. W. Terry, *Phys. Rev. Lett.* **72**, 2565 (1994).

¹⁶J. D. Murray, *Mathematical Biology: I. An Introduction*, 3rd ed. (Springer, New York, 2002).

¹⁷C. S. Holling, *Can. Entomol.* **91**, 385 (1959).

¹⁸Z. Yan, G. R. McKee, R. J. Groebner, P. B. Snyder, T. H. Osborne, M. N. Beurskens, and K. H. Burrell, *Phys. Plasmas* **18**, 056117 (2011).